Research Article Vol. 2, No. 4 / 15 April 2019 / OSA Continuum 1028

Single-longitudinal-mode diamond laser stabilization using polarization-dependent Raman gain

SOUMYA SARANG,[1,*] ONDREJ KITZLER,[1] OLIVER LUX,[2] ZHENXU BAI,[1,3] ROBERT J. WILLIAMS,[1] DAVID J. SPENCE,[1] AND RICHARD P. MILDREN[1]

[1]*MQ Photonics Research Centre, Department of Physics and Astronomy, Macquarie University, NSW 2109, Australia*
[2]*Now at Deutsches Zentrum für Luft- und Raumfahrt (DLR), Institut für Physik der Atmosphäre, 82234 Weßling-Oberpfaffenhofen, Germany*
[3]*National Key Laboratory of Science and Technology on Tunable Laser, Harbin Institute of Technology, Harbin 150001, China*
[*]*soumya.soumya@hdr.mq.edu.au*

Abstract: We report a novel cavity feedback mechanism for stabilizing single-longitudinal-mode (SLM) operation of diamond Raman lasers. Polarization-dependent Raman gain and in-grown stress birefringence in diamond were investigated as sources for Hänsch-Couillaud-type locking signals. The power range of SLM operation increased from 2.1 W to 7.2 W, compared to the free-running laser, for a simple standing-wave laser cavity without frequency-selective elements. Methods for further increasing power range and frequency stability are discussed.

1. Introduction

Single-longitudinal-mode (SLM) lasers are critical for precision science, space and spectroscopic applications such as atom cooling [1], gravitational wave sensing [2], laser guide star [3], remote sensing [4], high-resolution spectroscopy and metrology [2,5]. Many of these applications impose stringent requirements on linewidth, operating wavelength, spectral tunability and output power. While solid-state SLM lasers provide a robust and often compact platform, they are typically limited in wavelength coverage and output power. Therefore, there is a need for powerful SLM sources at wavelengths outside the range provided by conventional inversion laser media (such as Ti:Sapphire, and Yb fibers), with superior compactness, robustness and output power over optical parametric oscillators. Raman lasers have been successfully implemented in expanding the spectral range of conventional inversion lasers; however, until recently only a few SLM Raman lasers have been demonstrated [6–13] and usually only by applying frequency-narrowing architectures such as ring cavities [8], etalons [9] or injection seeding [10,11] or by ensuring cavity mode spacing greater than the Raman gain bandwidth [12,13].

We recently reported a SLM diamond Raman laser (DRL) in a free-running standing-wave cavity by exploiting the absence of spatial-hole-burning in a Raman gain medium [14]. The free spectral range (FSR) of the Raman laser was 35 times smaller than the diamond gain bandwidth (45 GHz, full width at half-maximum). This demonstration raised the possibility for conceptually simple, high-power diamond Raman oscillators that are adaptable to a range of pumps, possibly including multimode pumps. The power range of stable SLM operation, up to 4 W, was ultimately limited by the coupling between the cavity length and output power via Stokes heating. Active cavity length compensation for the thermally-induced cavity length changes was recommended as a way to increase SLM power and also to enhance frequency stability.

#356009 https://doi.org/10.1364/OSAC.2.001028
Journal © 2019 Received 21 Dec 2018; revised 3 Mar 2019; accepted 4 Mar 2019; published 15 Mar 2019

OSA CONTINUUM

At present, there are several approaches to achieve laser wavelength stabilization, including side-of-fringe locking [15], Hänsch-Couillaud (HC) [16,17], Pound-Drever-Hall (PDH) [18] and mode-interference locking [19]. The HC method is a top-of-fringe method that is straightforward to implement, as it relies on passive polarization-dependent effects present in the cavity to generate a dispersion-like locking signal (derivative of the cavity resonance peak) [17]. Variants of the HC method have also been demonstrated which utilize an intracavity Brewster plate, a birefringent crystal [16,20] or birefringence in the cavity mirrors [21] to generate a locking signal. Recently, a 1 W SLM continuous-wave (CW) ring DRL was demonstrated at 883 nm through HC locking technique by enabling differential pump loss using Brewster-cut diamond [8].

Although diamond is a nominally isotropic crystal, it often possesses stress-induced birefringence due to grown-in defects during production [22] which in principle may provide an intrinsic polarization-dependent mechanism for cavity locking. In this paper, we investigate an HC-type method to actively stabilize a CW DRL operating at 1240 nm wavelength. A variant is proposed and demonstrated that does not rely solely on the crystal birefringence but on polarization-dependent pump depletion. To elucidate the locking mechanism, a theoretical modelling of the HC locking signal below and above Raman lasing threshold is presented. Finally, the factors contributing to the quality of the locking signal are discussed in this paper.

2. Experimental design and setup

The cavity stabilization setup for the DRL is shown in Fig. 1. The pump source was a CW tunable distributed feedback laser (TOPTICA Photonics, model DL DFB BFY) amplified by an Yb fiber amplifier (IPG Photonics, model YAR-LP-SF) providing 50 W of output power at 1064 nm wavelength with beam quality of $M^2 = 1.05$. The pump linewidth of 5 MHz, which was much narrower than the diamond Raman gain bandwidth (~45 GHz), ensured a homogenous Raman gain spectrum [14]. A half-wave plate was used to orient the pump polarization along the $<111>$ axis of diamond to access maximum Raman gain [23]. A convex lens of focal length 50 mm was placed in front of the input coupler to focus the pump beam into the centre of the diamond, resulting in a focal spot radius of 40 μm.

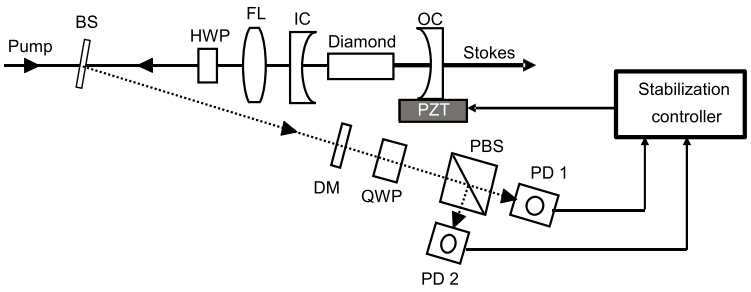

Fig. 1. Experimental arrangement of a cavity-locked DRL; BS - beam sampler, HWP - half-wave plate, FL - focusing lens, IC - input coupler, OC - output coupler, PZT - piezoelectric translation stage, DM - dichroic mirror, QWP - quarter-wave plate, PBS - polarizing beam splitter, PD1 and PD2- photodetectors.

The Raman laser consisted of 8×4×1.2 mm^3 low nitrogen, low-birefringence single-crystal diamond placed at the midpoint of a 102 mm long near-concentric cavity consisting of two 50 mm radius of curvature concave mirrors. The CVD-grown diamond was cut for propagation along the $<110>$ direction and had a stress-induced birefringence of approximately $\Delta n = 5 \times 10^{-6}$ at near-IR wavelengths (similar to that used in [24,25]). The input coupler was highly transmitting ($T = 99.26\%$) at the pump wavelength and highly reflective ($R = 99.94\%$) at the Stokes wavelength, whereas the output coupler was highly reflective ($R = 90\%$) at the pump wavelength and partially

OSA CONTINUUM

transmitting ($T = 0.5\%$) at the Stokes wavelength. The diamond end-faces were anti-reflection coated at the pump and Stokes wavelengths ($R < 1\%$ at 1064 nm, $R < 0.25\%$ at 1240 nm) to minimize intracavity losses.

A beam sampler reflected a part of the residual pump (after double-passing the DRL cavity) into the polarization analyzer comprising of a quarter-wave plate, polarizing beam splitter, and two silicon photodiodes. The quarter-wave plate was oriented to balance the incident pump power on the two photodetectors [17]. The difference between the two photodetector signals provided the locking signal for the PID controller (Laselock digital, TEM Messtechnik), which stabilized the Raman cavity length by driving the piezo-translation positioning stage (PZT, Thorlabs NFL5PD20) on which the output coupler was mounted. The maximum travel range of the PZT is 20 µm for an applied voltage of 0 to 75 V (provided by a Thorlabs controller).

The longitudinal mode spectrum of the output was investigated using a confocal scanning Fabry-Perot (FP) interferometer (Thorlabs, SA210) with 67 MHz resolution and FSR of 10 GHz. The output spectrum was also monitored using an optical spectrum analyzer (OSA; Anritsu, MS9710C) with a resolution of 0.05 nm. The centre wavelength stability was monitored using a laser spectrum analyzer (Bristol instruments, model 771A-NIR).

3. Calculated HC locking signal below and above Raman lasing threshold

In the HC-method, the zero-crossing of the dispersion-like locking signal is used to stabilize the laser cavity length to the centre of the resonance peak [17]. To analyze the locking signals and the stability below and above the Raman lasing threshold, locking signals were modelled using MATLAB. The starting point for the model is a cavity with birefringence as in Ref. [20] which calculates the reflected pump field $E^{r}_{x,y}$ as

$$E^{\mathrm{r}}_{x,y} = E^{\mathrm{i}}_{x,y}\left\{\sqrt{R_1} - \frac{T_1 F(\cos\delta_{\mathrm{e,o}} - F + \mathrm{i}\sin\delta_{\mathrm{e,o}})}{\sqrt{R_1}\left((1-F)^2 + 4F\sin^2\left(\delta_{\mathrm{e,o}}/2\right)\right)}\right\} \tag{1}$$

from the incident electric field $E^{\mathrm{i}}{}_{x,y}$, where $F = \sqrt{R_1 R_2 (1-L)^2}$ is the amplitude ratio per roundtrip accounting for two reflections at the input (R_1) and output mirrors (R_2) and intracavity losses (L), T_1 is the input mirror transmittance, and δ_{e} and δ_{o} are the phase changes of the extraordinary and ordinary ray, respectively. The amplitude of the detector signals (E_a and E_b) depend on the angle of the quarter-wave plate fast-axis with respect to the polarizer (θ) according to

$$\begin{pmatrix} E_a \\ E_b \end{pmatrix} = \begin{pmatrix} \cos\theta & -\sin\theta \\ \sin\theta & \cos\theta \end{pmatrix}\begin{pmatrix} 1 & 0 \\ 0 & \mathrm{i} \end{pmatrix}\begin{pmatrix} \cos(-\theta) & -\sin(-\theta) \\ \sin(-\theta) & \cos(-\theta) \end{pmatrix}\begin{pmatrix} E^{\mathrm{r}}_x \\ E^{\mathrm{r}}_y \end{pmatrix} \tag{2}$$

The locking signal is then the difference in the detector signals, $I_a - I_b \propto |E_a|^2 - |E_b|^2$. The absorption and crystal reflection losses were obtained from the laser threshold and slope efficiency calculation using the model described in [26], and were found to be 0.017%/mm and 0.1% per face, respectively. Using these values for the intracavity loss and R_1 and R_2 at the pump wavelength, F is calculated to be 0.08. The dephasing (Δ) per round trip induced by the birefringence (Δn) is calculated as $\Delta = (2\pi/\lambda).\,\Delta n.\,2l \approx 0.5$rad, where l is the length of the diamond. By substituting these parameter values in Eqs. (1) and (2), the locking signal below the Raman lasing threshold was calculated, as shown in Fig. 2(a) when the Raman cavity length is scanned by a triangular ramp at a rate of 5 µm/s. It can be seen that the locking signal is sinusoidal and only slightly shifted with respect to the reflected pump resonance, thus not providing a suitable lock point at the steep side of the signal. Therefore, the diamond birefringence alone is found to be insufficient in this case to provide a suitable locking signal for cavity stabilization.

OSA CONTINUUM

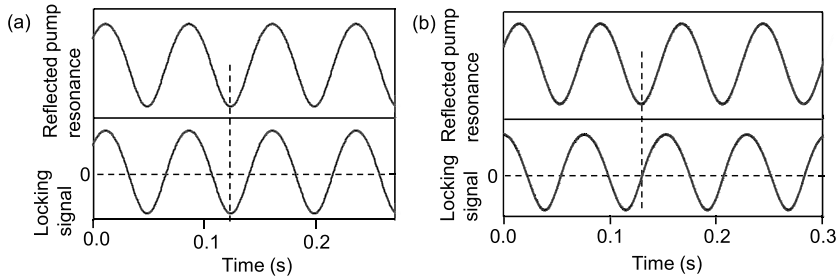

Fig. 2. Calculated locking and reflected pump signals at (a) below, and (b) above Raman lasing threshold when the cavity length is scanned at the rate of 5 µm/s. The vertical and horizontal lines indicate lock-point and zero-crossing for signal, respectively.

Above lasing threshold, the error-signal dynamics are anticipated to be more complex due to the Raman losses for each pump polarization component. These are captured in the four coupled differential equations for the orthogonal components of the pump and Stokes fields

$$\frac{\mathrm{d}S_k}{\mathrm{d}z} = \frac{g}{2}\sum_{\mathrm{ijl}} \chi_{ijkl} S_i P_j P_l^*, \tag{3a}$$

$$\frac{\mathrm{d}P_l}{\mathrm{d}z} = -\frac{g}{2\eta}\sum_{\mathrm{ijk}} \chi_{ijkl} S_i P_j S_k^*, \tag{3b}$$

where S and P are amplitudes of the Stokes and pump fields, respectively, g is the Raman gain coefficient of the Stokes wave, η is the quantum defect and χ is the normalized third-order nonlinear susceptibility with the indices i, j, k, and l referring to local x or y axes of a chosen basis. All other parameters such as beam sizes are normalized to 1. In general, χ has 16 coefficients relating to the interactions between the two Stokes and two pump fields. However, by choosing a basis with x being parallel to the $<110>$ and y being parallel to the $<100>$ direction in diamond, only five coefficients are non-zero and equal to 1, thus simplifying the equations to

$$\frac{\mathrm{d}S_x}{\mathrm{d}z} = \frac{g}{2}(S_x P_x P_x^* + S_x P_y P_y^* + S_y P_x P_y^*) \tag{4a}$$

$$\frac{\mathrm{d}S_y}{\mathrm{d}z} = \frac{g}{2}(S_y P_x P_x^* + S_x P_y P_x^*) \tag{4b}$$

$$\frac{\mathrm{d}P_x}{\mathrm{d}z} = -\frac{g}{2\eta}(S_x P_x S_x^* + S_x P_y S_y^* + S_y P_x S_y^*) \tag{4c}$$

$$\frac{\mathrm{d}P_y}{\mathrm{d}z} = -\frac{g}{2\eta}(S_y P_x S_x^* + S_x P_y S_x^*). \tag{4d}$$

When depletion is negligible (ie., near threshold), the polarization of the Stokes aligns itself to the angle providing the highest gain for the given linear pump polarization (in the absence of birefringence [25]). This is found by maximizing S^2 from Eqs. (4a) and (4b), a calculation equivalent to that for the scattering intensity given in [23]. Well above laser threshold, however, the polarization dependence of Raman gain (gain anisotropy) causes pump field components to be inhomogeneously depleted. Thus, the pump polarization effectively rotates as it propagates through the crystal thus providing an additional mechanism for cavity locking. The rotation effect is shown in Fig. 3 for the cases of threshold and with 50%, 70%, 90% and 99% depletion of the pump. Rotation occurs for all pump polarizations unless parallel to 35.3° ($<111>$ direction in diamond) or at 90° (assuming negligible birefringence). The model also provides the Stokes

OSA CONTINUUM

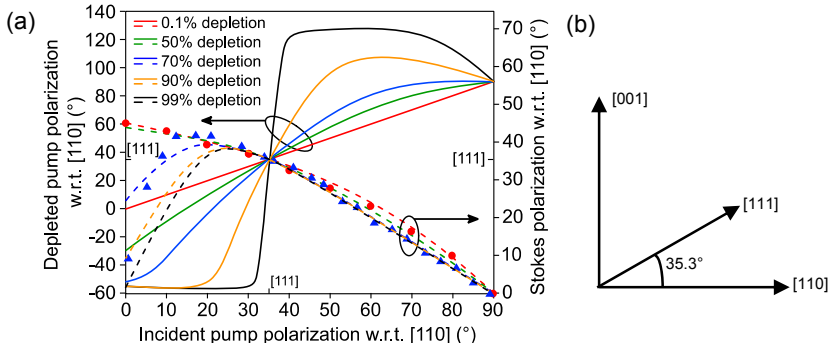

Fig. 3. (a).Polarization angle of Stokes output (dashed lines) and depleted pump (solid lines) as a function of incident pump polarization angle. Red, green, blue, orange and black lines are modeled dependencies for 0.1%, 50%, 70%, 90% and 99% depletion, respectively. Blue triangles are data from [23] while red circles are data from this study. (b).Crystallographic directions in the plane normal to propagation.

output polarizations (RH axis) which agrees with measurements for lasers operating near and well above threshold [23].

In CW DRLs of the type used in this study, the Stokes polarization is sensitive to the presence of birefringence and is oriented along the axes of local birefringence, rather than the usual case of orienting itself at the direction providing highest gain [25]. Even for pump polarization aligned to <111> (or <100>) crystallographic directions, if the Stokes polarization is not aligned to its high gain direction due to birefringence, the pump has an additional rotation mechanism due to the anisotropic Raman gain. Figure 4 shows an example solution of depleted pump polarization at an initial angle of 35.3° as a function of depletion for different fixed Stokes orientations. This shows that the depleted pump polarizations rotate, except for Stokes polarization angles parallel to [111] and [110] directions.

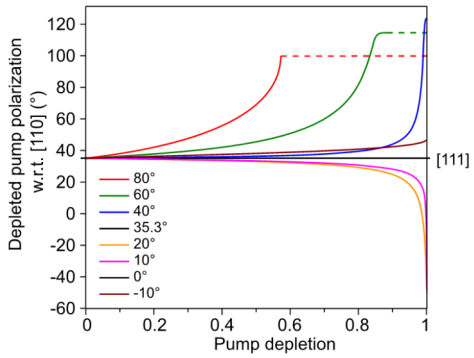

Fig. 4. Depleted pump rotation as a function of pump depletion for fixed Stokes angle between −10° and 80°. For Stokes angles above 40°, the depletion rate of the pump decreases significantly after reaching a steady state angle, shown as dashed lines.

In order to estimate the contribution of the pump rotation towards the HC locking signal above the Raman laser threshold, we calculated the locking signal corresponding to pump depletion for components along x and y axes. For this purpose, we considered conditions as shown in Fig. 4 for 50% depletion and fixed Stokes angle at 60°. The pump in this case rotates from 35.3° to 45.6° due to the disparate depletion of the x and y axis components (by 57% and 38%, respectively).

OSA CONTINUUM

In order to calculate the expected contribution to the locking signal above threshold, additional depletion factors are included in the amplitude ratio term F for the e-ray and o-ray, giving

$$F_{x,y} = \sqrt{R_1 R_2 (1-L)^2 (1-F_{lossx,y})^2} \tag{5}$$

where $F_{\mathrm{loss,x}}$ and $F_{\mathrm{loss,y}}$ are the depletion rates of the x and y polarization components of the pump. Thus, Eq. (1) for the reflected pump fields above threshold becomes

$$E^{\mathrm{r}}_{x,y} = E^{\mathrm{i}}_{x,y} \left\{ \sqrt{R_1} - \frac{T_1 F_{x,y} (\cos\delta_{\mathrm{e,o}} - F_{x,y} + \mathrm{i}\sin\delta_{\mathrm{e,o}})}{\sqrt{R_1}\left((1-F_{x,y})^2 + 4F_{x,y}\sin^2\left(\delta_{\mathrm{e,o}}/2\right)\right)} \right\}. \tag{6}$$

By substituting modeled values of 0.57 and 0.38 as $F_{\mathrm{loss,x}}$ and $F_{\mathrm{loss,y}}$ in Eq. (5) respectively, the locking signal was calculated using Eqs. (6) and (2). In contrast to the case for below Raman threshold, the modeling showed a phase shift in the calculated locking signal with respect to the pump resonance, such that the minimum of the reflected pump coincided with the steep section of the locking signal. When the quarter-wave plate orientation is altered from 45° to 68°, a zero-crossing signal is obtained as shown in Fig. 2(b). Though the locking signal is sinusoidal instead of the dispersion-like, as commonly seen in stabilization experiments, the pump-rotation mechanism is still capable of providing a lock as long as the peak of the resonance coincides with a steeply varying part of the locking signal [27]. Thus, the model indicates the feasibility of locking above laser threshold due to the polarization rotation provided by the polarization-dependent properties of the Raman gain.

The above calculation was carried out for present experimental case of <110> beam propagation; however, the principles could be readily applied to other propagation directions by applying the appropriate Raman susceptibility terms in Eqs. (3a) and (3b).

4. Results

The laser performance was first characterized without cavity length stabilization to provide a baseline. Above a threshold pump power of 23 W, the Stokes power increased linearly with a slope of 70% (Fig. 5). The residual pump power decreased monotonically with increasing incident pump power above the threshold for Stokes lasing, a feature which we find is important for generating SLM. The spectrum was SLM for output powers up to 2.1 W and transitioned to multimode operation thereafter. Moreover, the output beam was TEM_{00} for all Stokes powers. These observations are consistent with that reported previously for an unstabilized DRL in [14].

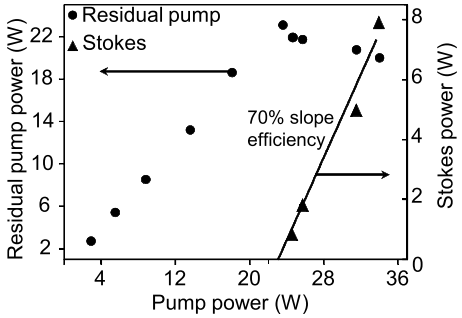

Fig. 5. Stokes power (triangles) and residual pump power (circles) characteristics without cavity stabilization.

Cavity stabilization was attempted at pump powers below the Raman lasing threshold. It can be seen from the Fig. 6(a) that there is a negligible shift between the peak of the transmitted

pump resonance and minimum of the locking signal suggesting that the phase shift induced by the diamond birefringence is too small to obtain a proper zero-crossing locking signal for cavity stabilization. The basic features of the experimental locking signal, which is scanned repeatedly over 1.8 times the cavity FSR, agree well with the model prediction in Fig. 2(a). Correspondingly, no stabilization was achieved.

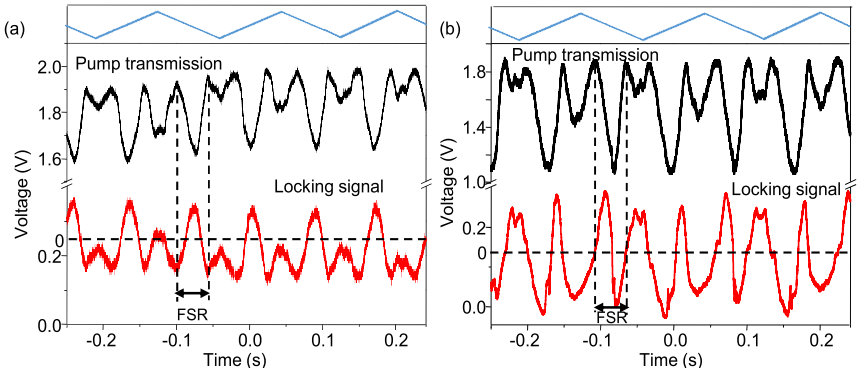

Fig. 6. Time traces of pump resonances (black) and locking signal (red) (a) below and (b) above laser threshold when the cavity length is scanned at the rate of 10 µm/s. The vertical and horizontal lines indicate lock-point and zero-crossing for signal, respectively. The trace (blue) above each figure indicates the timing of the voltage ramp.

Above laser threshold, a locking signal was generated with a steep edge coinciding with the peak of the pump transmission resonance [Fig. 6(b)], indicating a suitable lock-point as predicted in Fig. 2(b). SLM output was obtained at powers up to 7.2 W (see Fig. 7) for periods of a few seconds. The duration of stable SLM operation improved to several minutes when operating at a Stokes power level of 4.5 W. The laser operated at approximately same efficiency as running on multiple longitudinal modes.

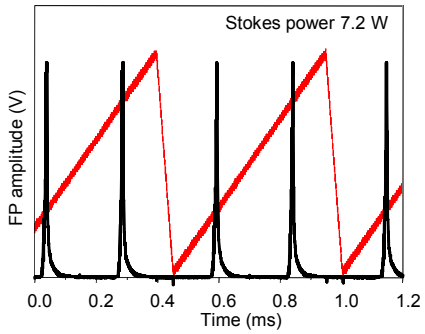

Fig. 7. FP scan (red) of the stabilized laser shows SLM operation (black) at 7.2 W Stokes power.

To further investigate stability, the Stokes central wavelength was monitored using the laser spectrum analyzer for a period of 3 minutes. As shown in Fig. 8(a), the wavelength fluctuated within a range of 125 MHz for 2 minutes and after this duration, the fluctuations increased for several seconds. The FP scan in Fig. 8(b) confirms that SLM was obtained for periods of up to 2 minutes and the output power was also stable during this period as indicated by the red line above longitudinal modes. The output then transitioned to multimode regime and the amplitude

OSA CONTINUUM

stability decreased as shown in Fig. 8(c). The laser often spontaneously reverted back to SLM (not shown in the figure) but the period of SLM was generally much shorter unless the set-point and PID settings were re-optimized.

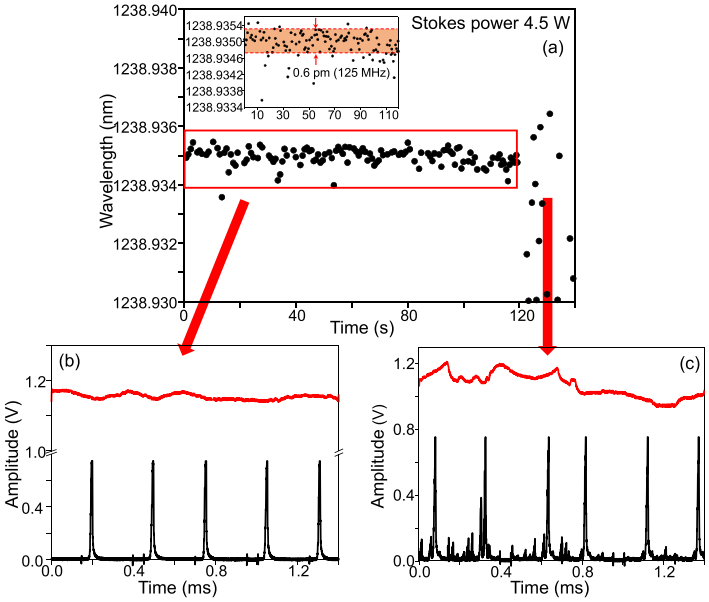

Fig. 8. (a) Stokes central wavelength fluctuations of the stabilized laser at 4.5 W power. The inset shows fluctuations in the output wavelength of about 125 MHz for about 2 mins. (b) FP scan of the laser output during the initial period. (c) FP scan of the laser output during de-stabilized operation, corresponding to the period after 120 seconds in (a). The red curves above the FP scans in (b) and (c) show the measured Stokes output power.

For higher output powers (> 5 W), the loss of locking was found to coincide with the deviation of the locking signal from the zero-level. In order to re-establish locking, the cavity length often required re-optimization of the set-point and PID settings. We attribute the vulnerability of the system locking to a combination of a small feedback bandwidth and some drift in pointing stability on the detectors. The slew rate of the PZT stage was 154 Hz (based on manufacturer specifications), thus suitable only for compensating for low frequency perturbations. The response time of the stage was further reduced by the additional mass of the output coupler mount. Usually a kHz bandwidth piezo stage is desired in such servo-loops [28]. Perhaps more critically, the detector signals were susceptible to pump beam pointing variations due to small drifts in cavity alignment. This problem directly affected the locking signal offset and hence was the likely cause of the need to re-optimize the setpoint. Improvement in the piezo-mount design (eg., by placing the piezo element on the mirror) and improving the imaging of the beam to the photodetectors is expected to greatly enhance stability and reduce sensitivity to perturbations.

5. Analysis and discussion

We have shown that HC cavity locking is possible above the laser threshold due to the polarization-dependent loss characteristics to the pump by the Raman process. The unstabilized DRL in the Ref. [14] reported an SLM output power of 4 W which was stable for a few tens of seconds. The experimental results show that the active stabilization of cavity length increased the maximum SLM power from 4 W to 7.2 W and, increased the stability period at the 4 W output power from few tens of seconds to 120 s. However, the slope of the locking signal at the lock-point

OSA CONTINUUM

was low; hence the locking was fundamentally less stable than typically obtained in HC locking. The criterion for a suitable locking signal is that the steep side of the calculated locking signal coincides with the dip/peak of the pump resonance. It is expected that improved locking may be achieved by enhancing either the effects of birefringence or Raman gain polarization-dependent through increasing the cavity finesse at the pump wavelength. We calculated locking signals for higher input reflectivities (R_1 = 10%, 30%, 50%, 70% and 90%) for the same birefringence and output reflectivity as used in the experiment. Using Eqs. (1) and (6) corresponding to the cases of below and above Raman threshold, respectively, the calculated locking signals are shown in Fig. 9(a) and (b) respectively, to compare the quality of each locking signal.

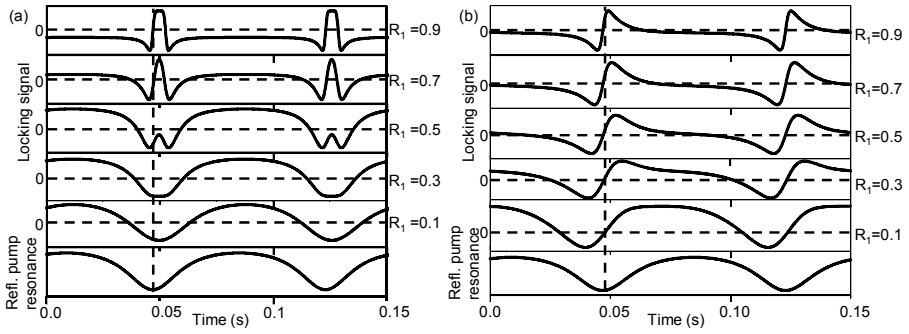

Fig. 9. Calculated locking signal for (a) below (b) above Raman threshold (for 50% depletion of the pump) for input mirror reflectivities R_1 = 10%, 30%, 50%, 70% and 90%, respectively. The vertical and horizontal lines indicate lock-point and zero-crossing for signal, respectively.

It is seen from Fig. 9(a) that, for the model based purely on HC locking due to birefringence, suitable lock-points are predicted for R_1 = 70% and beyond. A significant inference obtained from these theoretical plots is that even though the birefringence-induced dephasing is low, it is sufficient when using a cavity of modest finesse, in agreement with the findings in Ref. [29]. Figure 9(b) shows that much greater enhancements to the lock signal are obtained above laser threshold. Dispersion-like signals more familiar with the conventional HC method are produced when using 10% and higher reflectivities (assuming 50% pump depletion) with the dispersion shape more pronounced as finesse increases.

Rather than increasing finesse, increasing stability may be achieved by selecting diamond crystals with higher birefringence. In order to determine the birefringence value required to produce a usable locking signal for current cavity finesse below Raman threshold, a calculation using Eq. (1) was performed. As shown in Fig. 10, as birefringence increases, suitable lock-points are achieved for both 1.6 rad and 3.02 rad round-trip dephasing induced by birefringence levels of 1.7×10^{-5} and 3.2×10^{-5}, respectively. Therefore, a usable zero-crossing locking signal is produced in the low finesse Raman cavity if the diamond birefringence is 10 times higher than the present crystal birefringence. This may be feasible, for example, by using samples with a higher degree of in-grown stress-induced birefringence [22] or possibly by applying external stress to the crystal.

The use of a Brewster-cut diamond provides a further alternative for providing stabilization as demonstrated in [8] for a ring cavity resonant for the pump field as well as Stokes. In this case, the reflection losses at the Brewster surfaces provide the primary polarization-dependent loss mechanism that underpins the HC-stabilization scheme. Such an approach is feasible for the present standing-wave design, however, this would lead to a large increase in threshold due to the lateral expansion of the beams in the crystal (by a factor of the refractive index ~2.4) and due to

OSA CONTINUUM

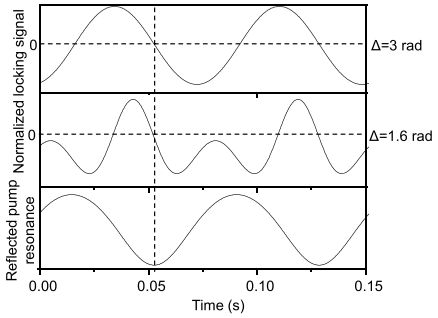

Fig. 10. Calculated locking signals and pump resonance for round-trip dephasing values of 1.6 and 3.02 rad. The vertical and horizontal lines indicate lock-point and zero-crossing for signal, respectively.

an increase in cavity losses in the presence of crystal birefringence. Hence, Brewster crystals may provide benefits in the case of higher power pumps.

Whereas increasing cavity Q is likely to increase stability in the present device, there are fundamental advantages to reduce Q. For example, it was recently shown that stable SLM operation from standing-wave diamond laser can be achieved using multimode pumps [30], which would be incompatible with a pump resonant scheme. This result highlights a potential route to stabilized cavities through a cavity locking mechanism based on the resonant Stokes field (for example, using a reference cavity or by injection locking with a low-power narrowband laser).

6. Conclusion

A variant of the Hänsch-Couillaud stabilization technique was investigated for a first Stokes DRL based on polarization-dependent Raman gain. In order to elucidate the stabilization mechanism, an analytical model was developed to generate the locking signals below and above Raman lasing threshold. An increase in the maximum SLM output power from 2.1 W to 7.2 W output power was demonstrated for the simple arrangement of an otherwise empty standing-wave cavity. We found that an increase in either the diamond birefringence or cavity finesse is required when using this technique to achieve SLM operation at higher output powers and over longer periods, and have suggested alternative locking methods for enhancing stability.

Funding

Australian Research Council (ARC) (DP130103799); Air Force Research Laboratory (AFRL) (FA2386-15-1-4075).

References

1. T. W. Hänsch and A. L. Schawlow, "Cooling of gases by laser radiation," Opt. Commun. **13**(1), 68–69 (1975).
2. J. Aasi, B. Abbott, R. Abbott, T. Abbott, M. Abernathy, K. Ackley, C. Adams, T. Adams, P. Addesso, and R. Adhikari, "Advanced ligo," Class. Quantum Gravity **32**(11), 115012 (2015).
3. D. B. Calia, Y. Feng, W. Hackenberg, R. Holzlöhner, L. Taylor, and S. Lewis, "Laser development for sodium laser guide stars at ESO," The Messenger **139**, 12–19 (2010).
4. D. T. Cassidy and L. J. Bonnell, "Trace gas detection with short-external-cavity InGaAsP diode laser transmitter modules operating at 1.58 μm," Appl. Opt. **27**(13), 2688–2693 (1988).
5. N. Bobroff, "Recent advances in displacement measuring interferometry," Meas. Sci. Technol. **4**(9), 907–926 (1993).
6. H. Rong, R. Jones, A. Liu, O. Cohen, D. Hak, A. Fang, and M. Paniccia, "A continuous-wave Raman silicon laser," Nature **433**(7027), 725–728 (2005).
7. C. Lee, C. Chang, P. Tuan, C. Cho, K. Huang, and Y. Chen, "Cryogenically monolithic self-Raman lasers: observation of single-longitudinal-mode operation," Opt. Lett. **40**(9), 1996–1999 (2015).

OSA CONTINUUM

8. O. Kitzler, J. Lin, H. M. Pask, R. P. Mildren, S. C. Webster, N. Hempler, G. P. Malcolm, and D. J. Spence, "Single-longitudinal-mode ring diamond Raman laser," Opt. Lett. **42**(7), 1229–1232 (2017).
9. Z. Liu, S. Men, Z. Cong, Y. Liu, H. Rao, S. Zhang, and X. Zhang, "Single-frequency Nd: GGG/$BaWO_4$ Raman laser emitting at 1178.3 nm," in CLEO: Sci. Innov., (Optical Society of America, 2016), SM3M. 3.
10. O. Lux, H. Fritsche, and H. J. Eichler, "Trace Gas Remote Sensing by Lasers," Opt. Photonik **8**(4), 48–51 (2013).
11. S. M. Spuler and S. D. Mayor, "Raman shifter optimized for lidar at a 1.5 μm wavelength," Appl. Opt. **46**(15), 2990–2995 (2007).
12. J. Brasseur, K. Repasky, and J. Carlsten, "Continuous-wave Raman laser in H_2," Opt. Lett. **23**(5), 367–369 (1998).
13. P. Latawiec, V. Venkataraman, M. J. Burek, B. J. M. Hausmann, I. Bulu, and M. Lončar, "On-chip diamond Raman laser," Optica **2**(11), 924–928 (2015).
14. O. Lux, S. Sarang, O. Kitzler, D. J. Spence, and R. P. Mildren, "Intrinsically stable high-power single longitudinal mode laser using spatial hole burning free gain," Optica **3**(8), 876–881 (2016).
15. O. Mhibik, T. H. My, D. Pabœuf, F. Bretenaker, and C. Drag, "Frequency stabilization at the kilohertz level of a continuous intracavity frequency-doubled singly resonant optical parametric oscillator," Opt. Lett. **35**(14), 2364–2366 (2010).
16. M. Vainio, J. E. Bernard, and L. Marmet, "Cavity-enhanced optical frequency doubler based on transmission-mode Hänsch–Couillaud locking," Appl. Phys. B **104**(4), 897–908 (2011).
17. T. Hansch and B. Couillaud, "Laser frequency stabilization by polarization spectroscopy of a reflecting reference cavity," Opt. Commun. **35**(3), 441–444 (1980).
18. T. T.-Y. Lam, B. J. Slagmolen, J. H. Chow, I. C. Littler, D. E. McClelland, and D. A. Shaddock, "Digital laser frequency stabilization using an optical cavity," IEEE J. Quantum Electron. **46**(8), 1178–1183 (2010).
19. D. Shaddock, M. Gray, and D. McClelland, "Frequency locking a laser to an optical cavity by use of spatial mode interference," Opt. Lett. **24**(21), 1499–1501 (1999).
20. J. Boon-Engering, W. Van der Veer, E. Bente, and W. Hogervorst, "Stabilization of an optical cavity containing a birefringent element," Opt. Commun. **140**(4-6), 285–288 (1997).
21. P. Asenbaum and M. Arndt, "Cavity stabilization using the weak intrinsic birefringence of dielectric mirrors," Opt. Lett. **36**(19), 3720–3722 (2011).
22. I. Friel, S. Clewes, H. Dhillon, N. Perkins, D. Twitchen, and G. Scarsbrook, "Control of surface and bulk crystalline quality in single crystal diamond grown by chemical vapour deposition," Diamond Relat. Mater. **18**(5-8), 808–815 (2009).
23. A. Sabella, J. A. Piper, and R. P. Mildren, "1240 nm diamond Raman laser operating near the quantum limit," Opt. Lett. **35**(23), 3874–3876 (2010).
24. O. Kitzler, A. McKay, and R. P. Mildren, "Continuous-wave wavelength conversion for high-power applications using an external cavity diamond Raman laser," Opt. Lett. **37**(14), 2790–2792 (2012).
25. H. Jasbeer, R. J. Williams, O. Kitzler, A. McKay, S. Sarang, J. Lin, and R. P. Mildren, "Birefringence and piezo-Raman analysis of single crystal CVD diamond and effects on Raman laser performance," J. Opt. Soc. Am. B **33**(3), B56 (2016).
26. O. Kitzler, A. McKay, D. J. Spence, and R. P. Mildren, "Modelling and optimization of continuous-wave external cavity Raman lasers," Opt. Express **23**(7), 8590–8602 (2015).
27. P. Esherick and A. Owyoung, "Polarization feedback stabilization of an injection-seeded Nd: YAG laser for spectroscopic applications," J. Opt. Soc. Am. B **4**(1), 41–47 (1987).
28. T. C. Briles, D. C. Yost, A. Cingöz, J. Ye, and T. R. Schibli, "Simple piezoelectric-actuated mirror with 180 kHz servo bandwidth," Opt. Express **18**(10), 9739–9746 (2010).
29. A. Libson, N. Brown, A. Buikema, C. C. López, T. Dordevic, M. Heising, and M. Evans, "Simple method for locking birefringent resonators," Opt. Express **23**(3), 3809–3817 (2015).
30. X. Yang, O. Kitzler, D. J. Spence, R. J. Williams, Z. Bai, S. Sarang, L. Zhang, Y. Feng, and R. P. Mildren, "Single-frequency 620 nm diamond laser at high power, stabilized via harmonic self-suppression and spatial-hole-burning-free gain," Opt. Lett. **44**(4), 839–842 (2019).